Supporting Information

Enhancing the Electrocatalytic Activity of 2H-WS_2 for Hydrogen Evolution via Defect Engineering

Longfei Wu,[a] Arno J. F. van Hoof,[a] Nelson Y. Dzade,[b] Lu Gao,[a] Marie-Ingrid Richard,[c] Heiner Friedrich,[d] Nora H. De Leeuw,[b] Emiel J. M. Hensen[a] and Jan P. Hofmann[a]*

[a]*Laboratory for Inorganic Materials and Catalysis, Department of Chemical Engineering and Chemistry, Eindhoven University of Technology, P.O. Box 513, 5600 MB Eindhoven, The Netherlands*

[b]*Faculty of Geosciences, Utrecht University, P.O. Box 80.021, 3508 TA Utrecht, The Netherlands*

[c]*Laboratory of Materials and Interface Chemistry, Department of Chemical Engineering and Chemistry, Eindhoven University of Technology, P.O. Box 513, 5600 MB Eindhoven, The Netherlands*

[d]*Aix Marseille Université, CNRS, Université de Toulon, IM2NP UMR 7334, 13397, Marseille, France and ID01/ESRF, The European Synchrotron, 71 rue des Martyrs, Grenoble 38043 Cedex, France*

*Email address of corresponding author: J.P.Hofmann@tue.nl

TABLE OF CONTENTS

Part I: Material preparation

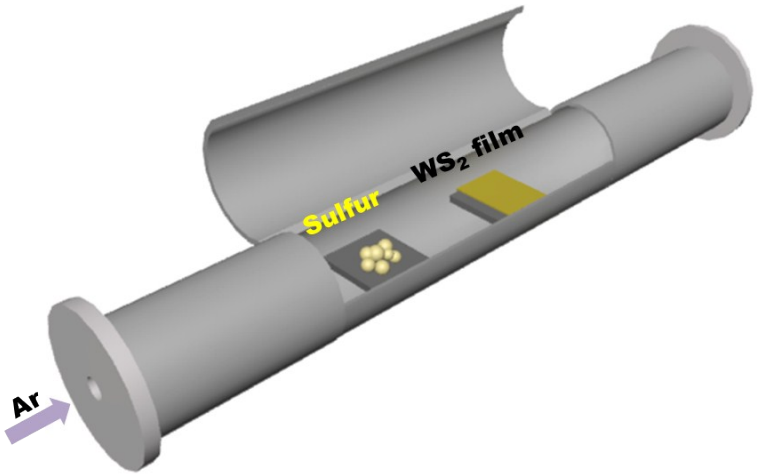

Figure S1. Schematic illustration of the tungsten sulfide preparation in thermal CVD setup.

Part II: X-ray crystallography

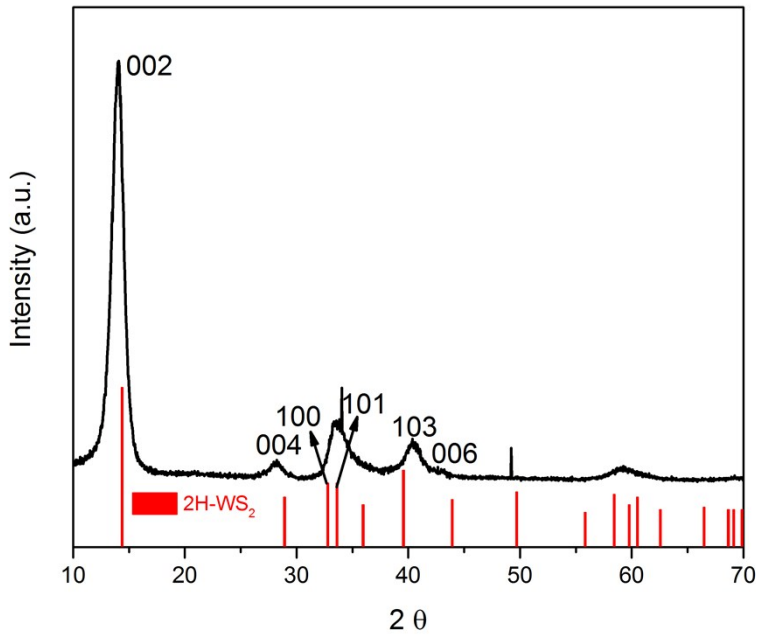

Figure S2. Grazing-incidence X-ray diffraction (GI-XRD) of a stoichiometric WS_2 film on SiO_2/Si substrate prepared at 600 ºC.

Part III: *In-situ* tracking of desulfurization

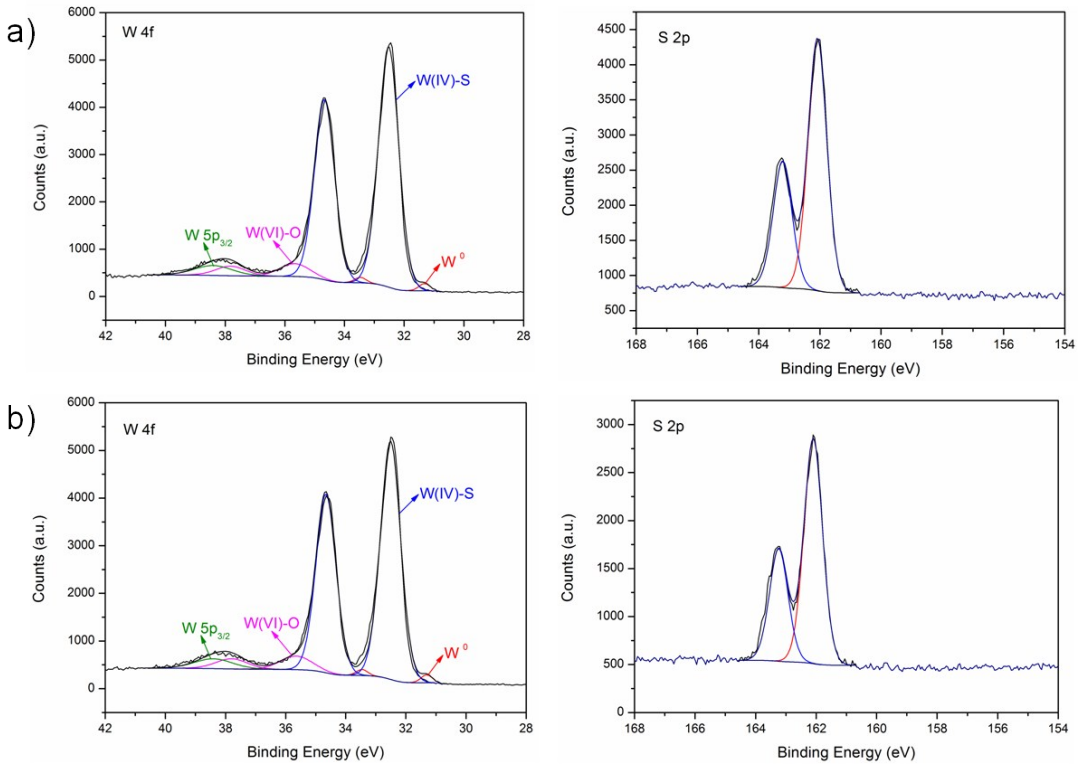

Figure S3. W 4f and S 2p X-ray photoelectron (XP) spectra of a tungsten sulfide film on SiO_2/Si before (a) and after annealing (b) in 5 mbar H_2 at 600 °C for 2 h.

Part IV: Defective tungsten sulfide

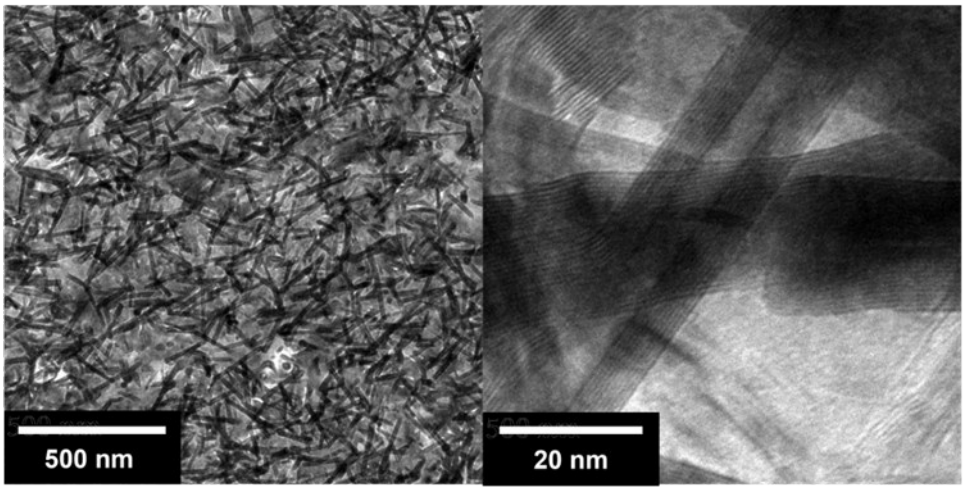

Figure S4. TEM image of $WS_{0.37}$ prepared at 600 °C.

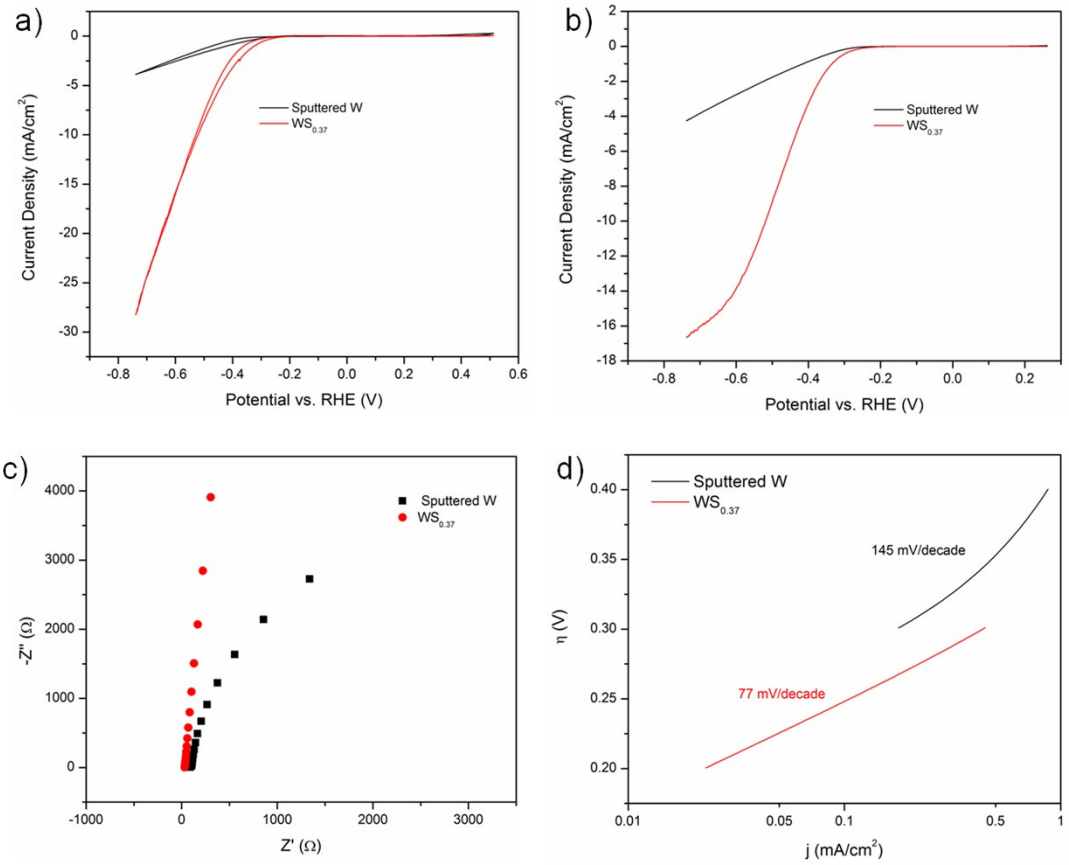

Figure S5. Cyclic voltammetry (a) and linear sweep voltammetry (b) curves of $WS_{0.37}$ and sputtered W in 0.5 M H_2SO_4, Scan rate: 50 mV/s for CV and 5 mV/s for LSV; c) Electrochemical impedance spectroscopy (EIS): Nyquist plots of $WS_{0.37}$ collected at open circuit potential in 0.5 M H_2SO_4 electrolyte with an AC amplitude of 10 mV; d) Tafel plots recorded with polarization curves shown in (b).

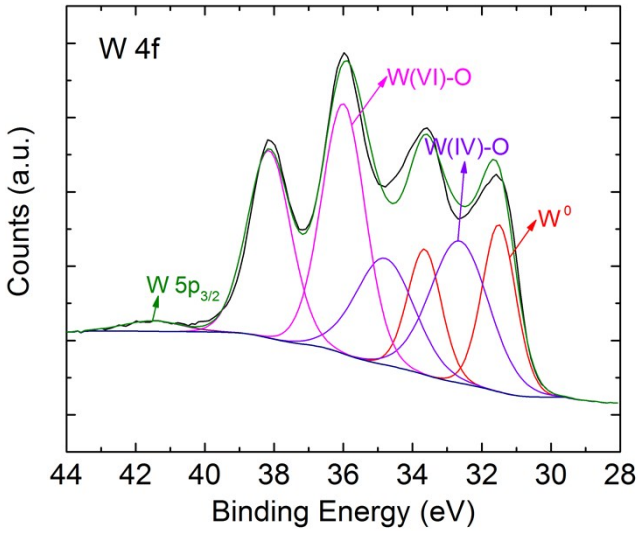

Figure S6. XP spectra of sputtered W on SiO_2/Si.

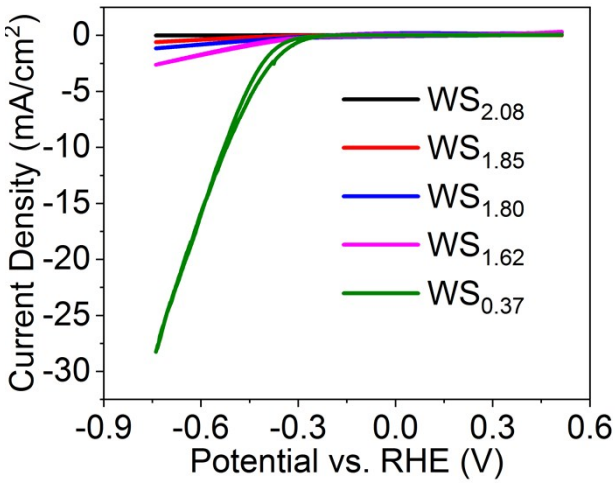

Figure S7. Cyclic voltammetry curves of as-prepared defective tungsten sulfide in 0.5 M H_2SO_4.

Scan rate: 50 mV/s.

Part V: H_2 annealing temperature variations

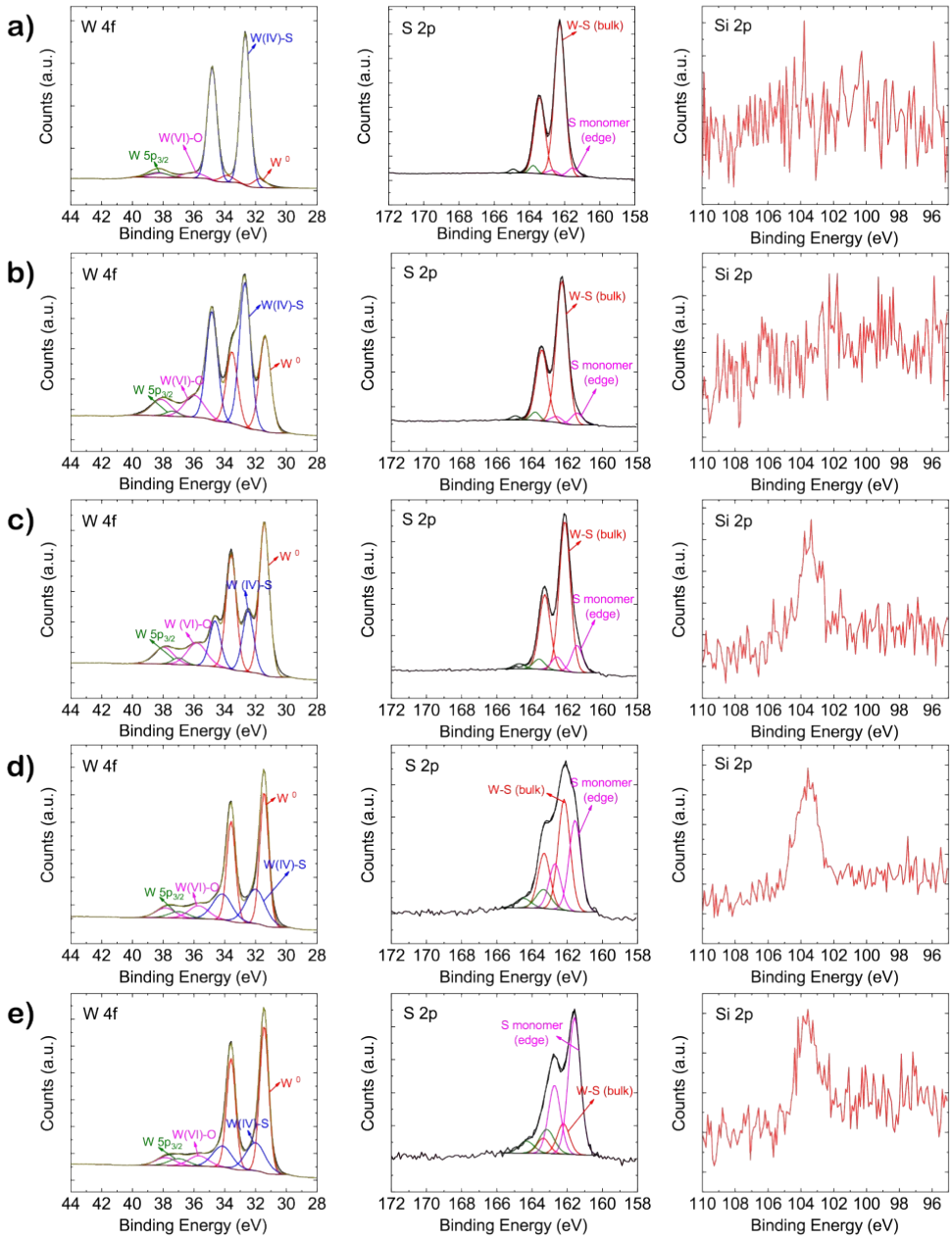

f)

Sample name	S/W ratio	S/W(IV)-S	% Atom W^0	% Atom WO_3	% Atom WS_2
WS_2	2.07	2.22	2.6	7.2	90.2
10 % H_2-0.5 h	2.03	2.30	7.2	6.4	86.4
10 % H_2-1 h	1.18	2.16	34.4	13.7	51.9
10 % H_2-1.5 h	0.48	1.78	58.3	16.3	25.4
10 % H_2-2 h	0.24	0.66	55.7	12.1	32.2
10 % H_2-3 h	0.17	0.54	63.6	9.9	26.5

Figure S8. a-e) XP spectra of tungsten sulfide films annealed in 10 % H_2 at 700 °C for 0.5 (a), 1 (b), 1.5 (c), 2 (d) and 3 (e) h; f) composition analysis of as-prepared tungsten sulfide films based on the XPS results.

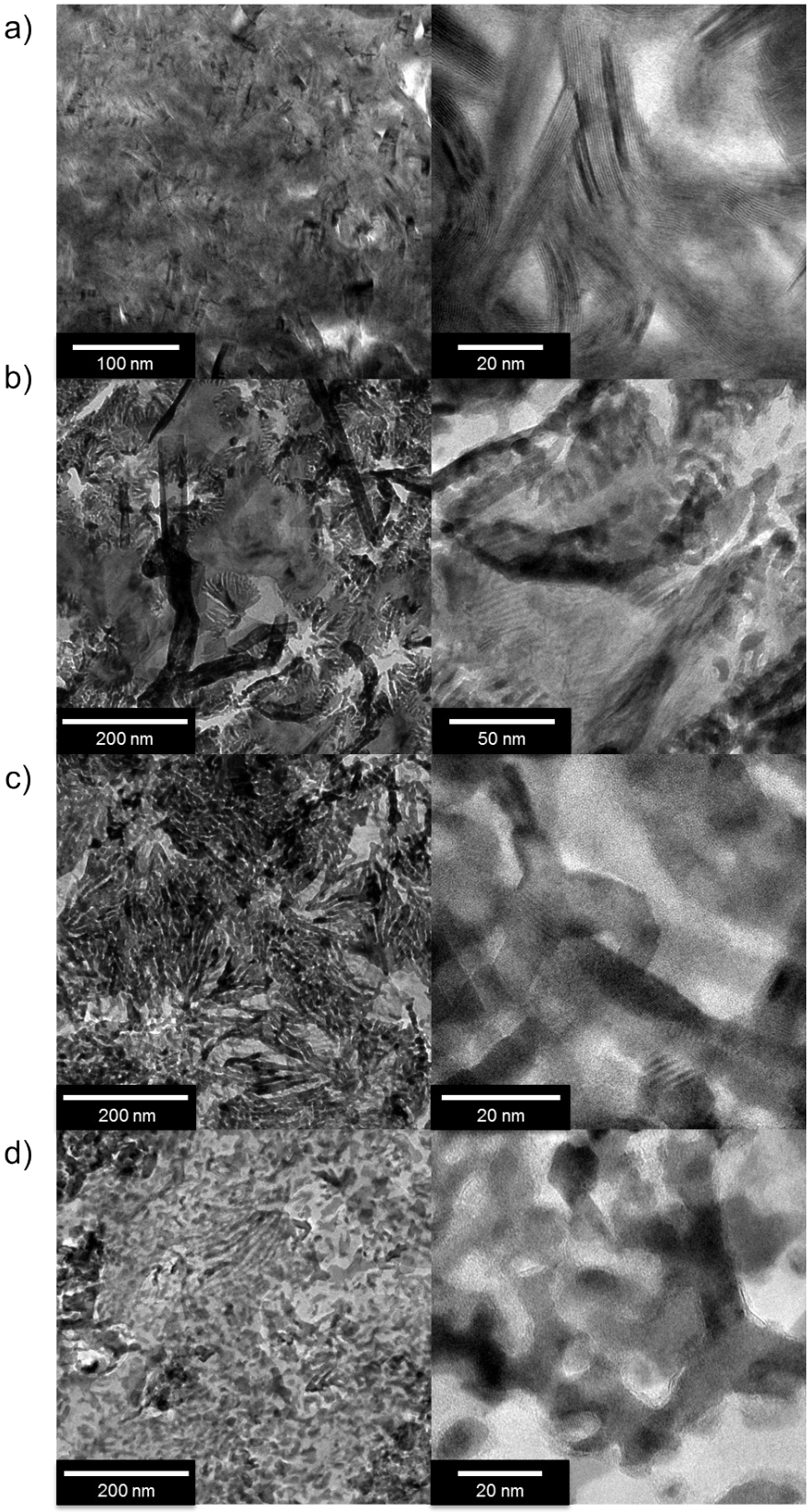

Figure S9. TEM images of tungsten sulfide films annealed in 10 % H_2 at 700 °C for 0 (a), 1 (b), 1.5 (c) and 3 h (d).

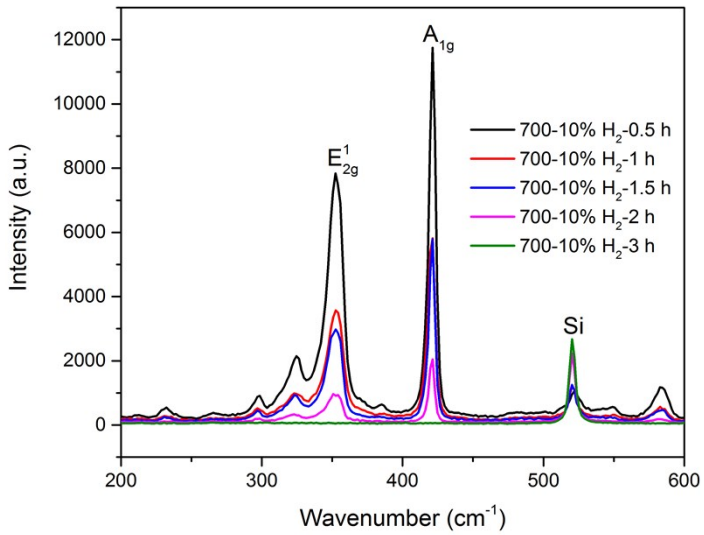

Figure S10. Raman spectra of tungsten sulfide films annealed in 10 % H_2 at 700 °C for different annealing times.

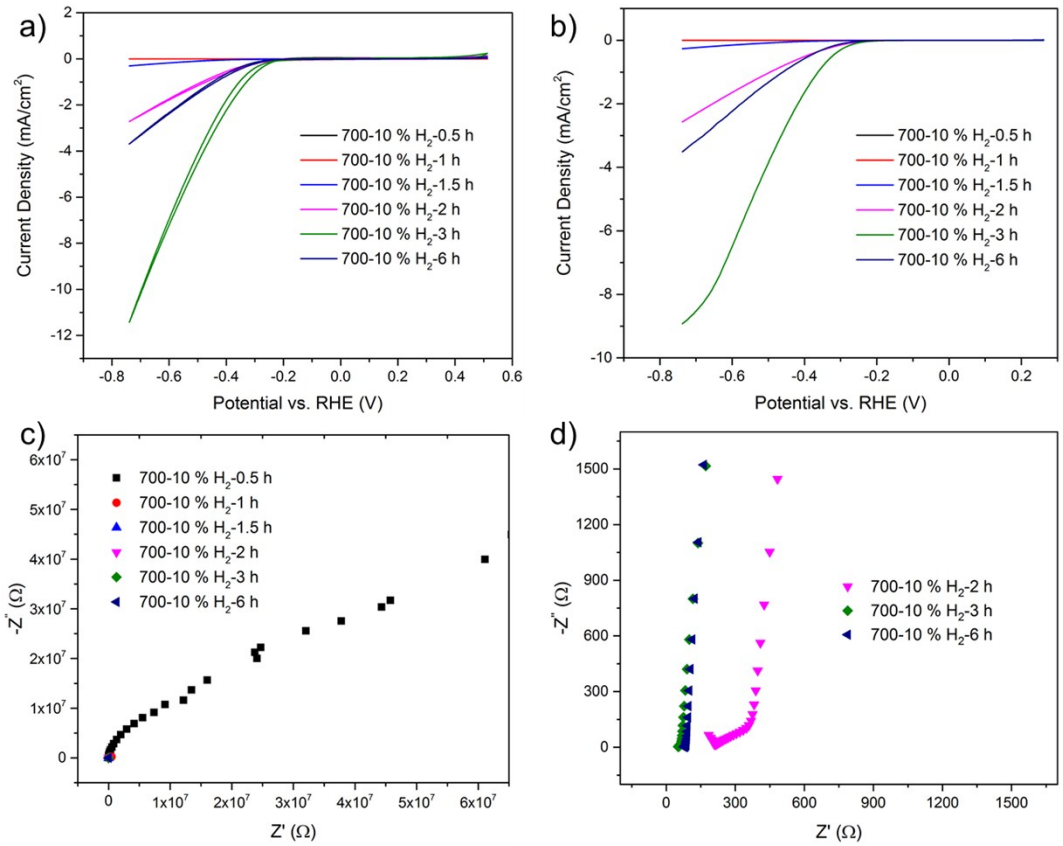

Figure S11. Cyclic voltammetry (a) and Linear sweep voltammetry (b) curves of WS_2 obtained after H_2 treatment in 10 % H_2 at 700 °C with different time in 0.5 M H_2SO_4, Scan rate: 50 mV/s for CV and 5 mV/s for LSV; c) Electrochemical impedance spectroscopy (EIS) Nyquist plots of as-prepared tungsten sulfide collected at open circuit potential in 0.5 M H_2SO_4 electrolyte with an AC amplitude of 10 mV; d) zoom-in Nyquist plots of tungsten sulfide films in c).

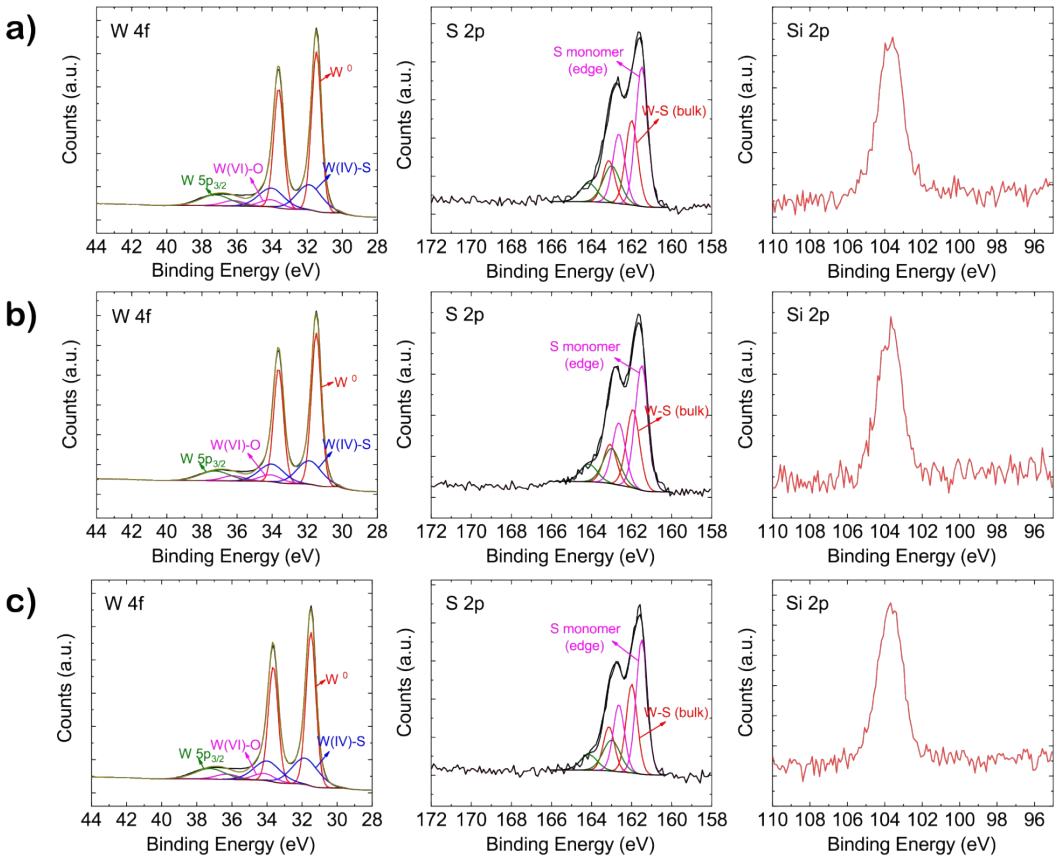

d)

Sample name	S/W ratio	S/W(IV)-S	% Atom W^0	% Atom WO_3	% Atom WS_2
WS_2	2.07	2.22	2.6	7.2	90.2
5 % H_2-3 h	0.16	0.42	66.1	6.8	27.1
5 % H_2-6 h	0.17	0.48	66.7	6.8	26.5
5 % H_2-10 h	0.14	0.39	63.7	6.5	29.8

Figure S12. a-c) XP spectra of tungsten sulfide films annealed in 5 % H_2 at 850 °C for 3 (a), 6 (b) and 10 (e) h; f) composition analysis of as-prepared tungsten sulfide films based on the XPS results.

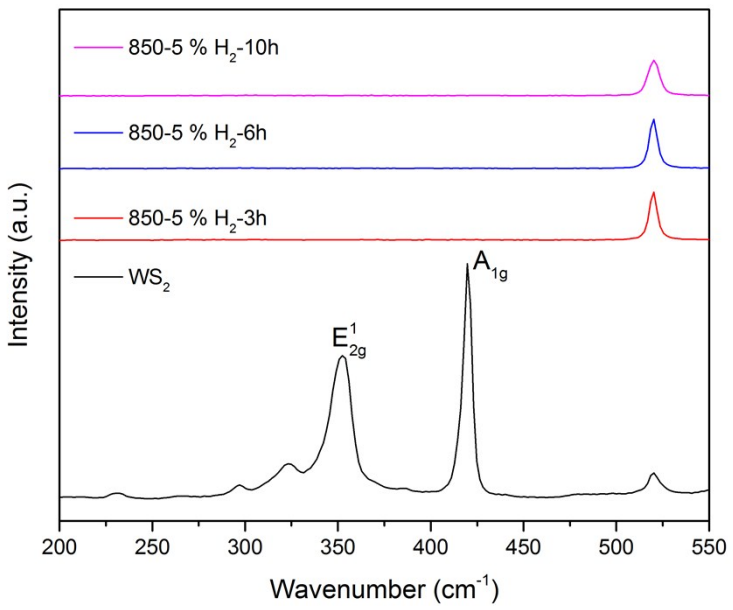

Figure S13. Raman spectra of tungsten sulfide films annealed in 5 % H_2 at 850 °C with different time.

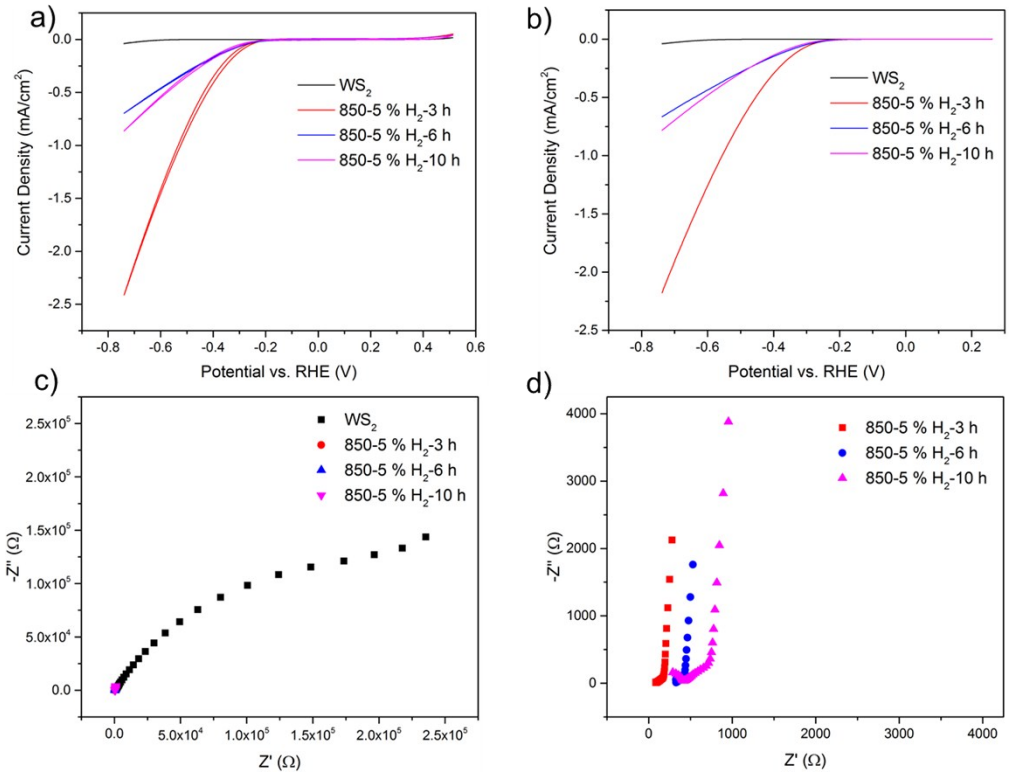

Figure S14. Cyclic voltammetry (a) and linear sweep voltammetry (b) curves of WS_2 obtained after H_2 treatment in 5 % H_2 at 850 °C with different time in 0.5 M H_2SO_4, Scan rate: 50 mV/s for CV and 5 mV/s for LSV; c) Electrochemical impedance spectroscopy (EIS) Nyquist plots of as-prepared tungsten sulfide collected at open circuit potential in 0.5 M H_2SO_4 electrolyte with an AC amplitude of 10 mV; d) zoom-in Nyquist plots of tungsten sulfide films in c).

Part VI: Structure and chemical analysis

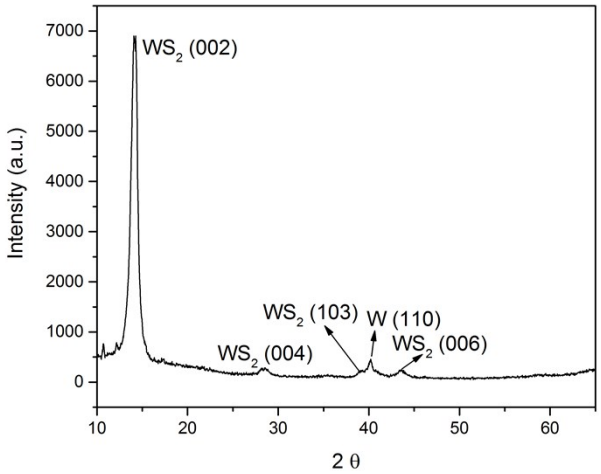

Figure S15. Nano-focus XRD pattern of $WS_{1.47}$ on SiO_2/Si beam recorded at a beam energy of 8 keV and beam size of 100×400 nm^2 indicating the presence of both WS_2 and W in the beam volume.

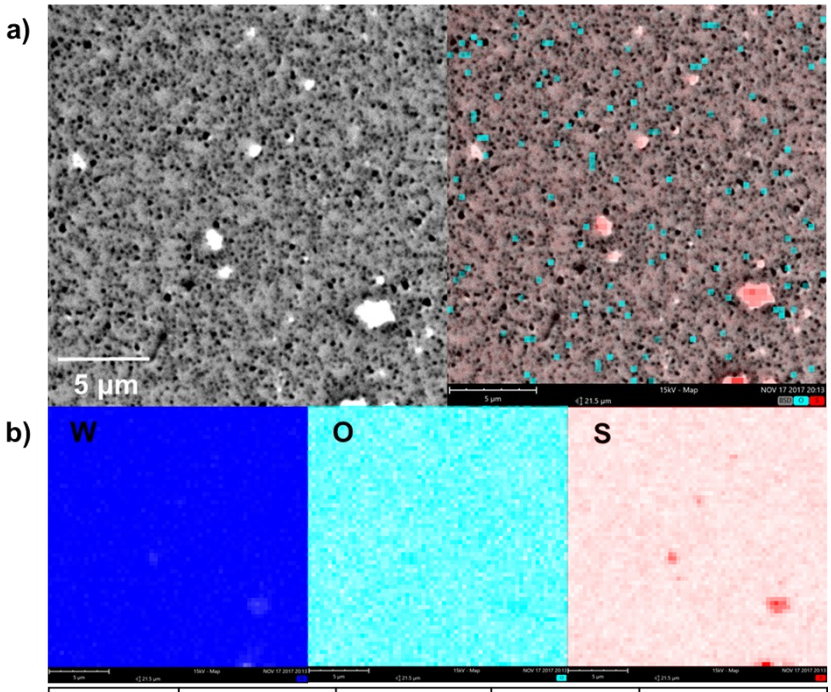

c)

Element Number	Element Symbol	Element Name	Atomic Conc. (%)	Weight Conc. (%)
74	W	Tungsten	54.0	92.0
8	O	Oxygen	38.3	5.7
16	S	Sulfur	7.7	2.3

Figure S16. a) SEM image (left) and merged EDX mapping for O (cyan) and S (red) of $WS_{0.95}$; b) EDX elemental mapping of $WS_{0.95}$ for W (blue), O (cyan) and S (red); c) elemental analysis of $WS_{0.95}$ based on EDX results.

Part VII: WS_{2-x} on Carbon Fiber Paper (CFP)

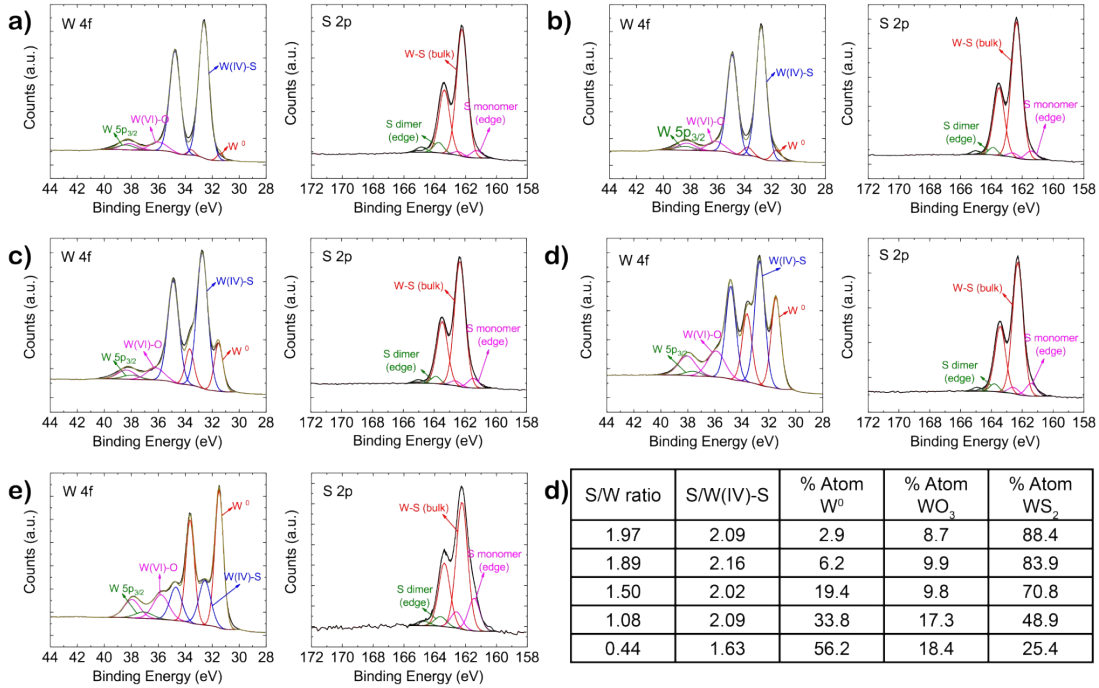

d)

S/W ratio	S/W(IV)-S	% Atom W^0	% Atom WO_3	% Atom WS_2
1.97	2.09	2.9	8.7	88.4
1.89	2.16	6.2	9.9	83.9
1.50	2.02	19.4	9.8	70.8
1.08	2.09	33.8	17.3	48.9
0.44	1.63	56.2	18.4	25.4

Figure S17. a-d) XP spectra of $WS_{1.97}$ (a), $WS_{1.89}$ (b), $WS_{1.50}$ (c), $WS_{1.08}$ (d) and $WS_{0.44}$ (e) on CFP; f) composition analysis of as-prepared tungsten sulfide films based on the XPS results.

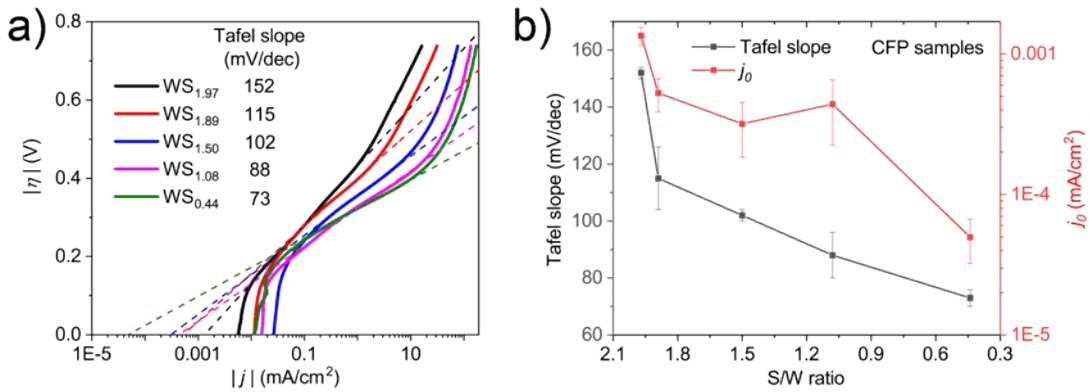

Figure S18. a) Tafel slopes obtained from LSV curves for tungsten sulfide on CFP; b) Plots of Tafel slope (black curve) and exchange current density (j_0) (red curve) values of tungsten sulfide on CFP substrates with decreasing S/W ratios.

The exchange current can be determined by back extrapolation of the Tafel region to the equilibrium potential. Therefore, we calculated both the current density and Tafel slope and plotted them versus S/W ratios, which is shown in Figure S18. However, the exchange current density (j_0) values decrease with smaller S/W ratios, which seems unrealistic as the Tafel slope indicates that the more defective tungsten sulfide has the higher HER activity. Therefore, we re-examined the method to determine j_0 and found a recent report that estimates of the "exchange current density" via back-extrapolation of the current from large overpotentials to the equilibrium potential may lead to different values depending on which HER step (Volmer, Heyrovsky or Tafel) is used.[1] It has also been pointed out in the same article that this approach may give unreliable values when used in regions where mass transport limitations or large Ohmic losses occur. Therefore, it might be more reasonable to evaluate the HER performances of the tungsten sulfide films based on Tafel slope values only.[2-4]

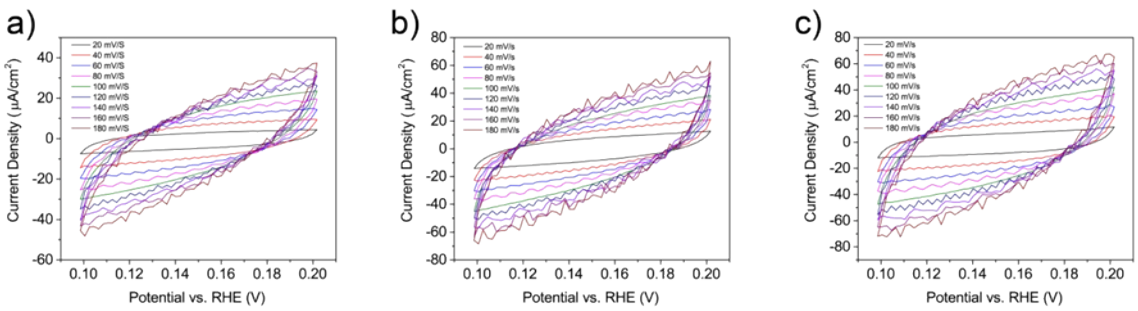

Figure S19. Cyclic voltammograms of the $WS_{1.97}$ (a), $WS_{1.08}$ (b) and $WS_{0.44}$ on carbon fiber paper (CFP) at various scan rates (20-180 mV/s) used to estimate the double layer capacitance (C_{dl}) and relative electrochemically active surface area.

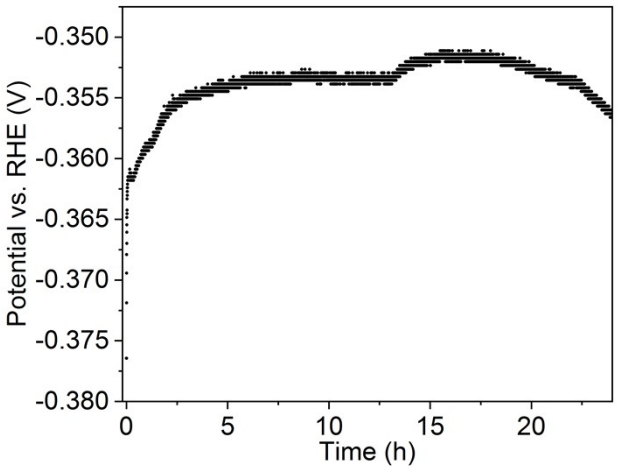

Figure S20. HER stability testing. Chronopotentiometric responses (V-t) recorded from $WS_{0.44}$ on CFP at a constant current density of 4.45 mA/cm^2.

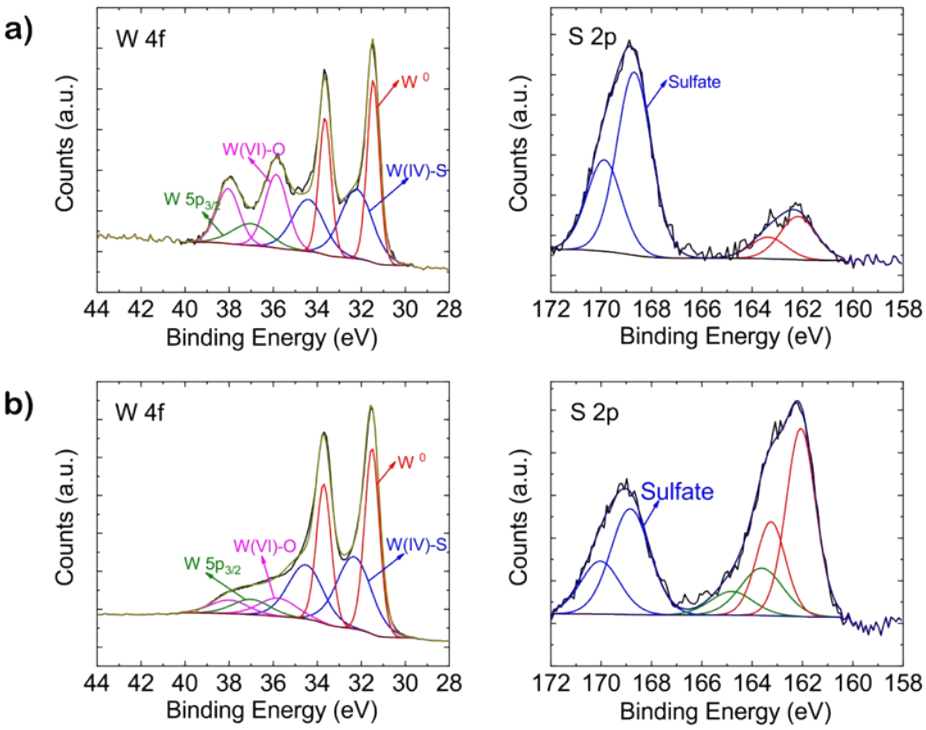

Figure S21. XP spectra of $WS_{0.44}$ on CFP after electrochemical stability test (a) and sputtered with Ar^+ ion gun for 10 cycles (estimated depth ~20 nm) (b).

Table S1. Summary of recently reported efficient WS_2-based HER electrocatalysts

Sample	Tafel slope (mV/decade)
Exfoliated 1T-WS_2 nanosheets[5]	55
Freeze-dried WS_2/rGO after annealing[6]	58
Ultra-thin WS_2 nanoflakes[7]	48
WS_2@P, N doped graphene[8]	53
WS_2 nanosheets from ball milling[9]	72
Highly defective $WS_{0.44}$ (*this work*)	60

Part VIII: Density Functional Theory (DFT) modeling

Computational Details

The first-principles calculations were performed by using the Vienna ab-initio simulation (VASP) package,[6,7] a periodic plane wave DFT code which includes the interactions between the core and valence electrons using the Projector Augmented Wave (PAW) method.[8,9] The electronic exchange–correlation potential was calculated using the GGA-PBE functional.[10] Wave functions were expanded in a plane wave basis with a high energy cutoff of 600 eV. The convergence criterion was set to 10^{-6} eV between two ionic steps for the self-consistency process, and 0.02 eV/ Å was adopted for the total energy calculations. A vacuum region of 15 Å was added along the normal direction to the monolayer to avoid interactions between adjacent images. The Brillouin zone was sampled sing an 8 × 8 × 1 Monkhorst-Pack *k*-point meshes, which were found to be sufficient to obtain well-converged results H-WS_2 systems. Van der Waals dispersion forces were accounted for in all calculations through the Grimme DFT-D3 functional,[11] which adds a semi-empirical dispersion potential to the conventional Kohn–Sham DFT energy.

We adopt the common used approach that hydrogen generation from electrochemical water splitting involves two reaction steps for the analysis of HER performance.[12,13] The HER is a classic example of a two-electron transfer reaction with one catalytic intermediate, H* (where * denotes a site on the surface able to bind to hydrogen), and may occur through either the Volmer-Heyrovsky ($H^+ + e^- + H^* \rightarrow H_2 + *$) or the Volmer-Tafel ($2H^* \rightarrow H_2 + 2*$) mechanism.[14] The free energy of $H^+ + e^-$ is the same as that of $1/2H_2$ at standard conditions.[12,13] The Gibbs free energy of hydrogen adsorption (ΔG_H), the best known descriptor for the hydrogen evolution activity was calculated by the free energy with respect to molecular hydrogen including zero-point energy and entropy terms via:

$$\Delta G_H = \Delta E_H + \Delta E_{ZPE} - T\Delta S_H \quad (1)$$

where ΔE_H is the adsorption energy of hydrogen which is defined as:

$$\Delta E_H = E_{WS_2+H} - E_{WS_2} - \frac{1}{2}E_{H_2} \quad (2)$$

The ΔE_{ZPE} in equation 1 is the difference in zero point energy between the adsorbed hydrogen and hydrogen in gas phase, and ΔS_H is the entropy difference between adsorbed state and gas phase. We

can take the entropy of atomic hydrogen as $\Delta S_H = -S_{H_2}/2$, where S_{H_2} is the entropy of molecule hydrogen in gas phase. Under standard conditions, $\Delta E_{ZPE} - T\Delta S_H$ is 0.24 eV, therefore $\Delta G_H = E_H + 0.24$ eV.

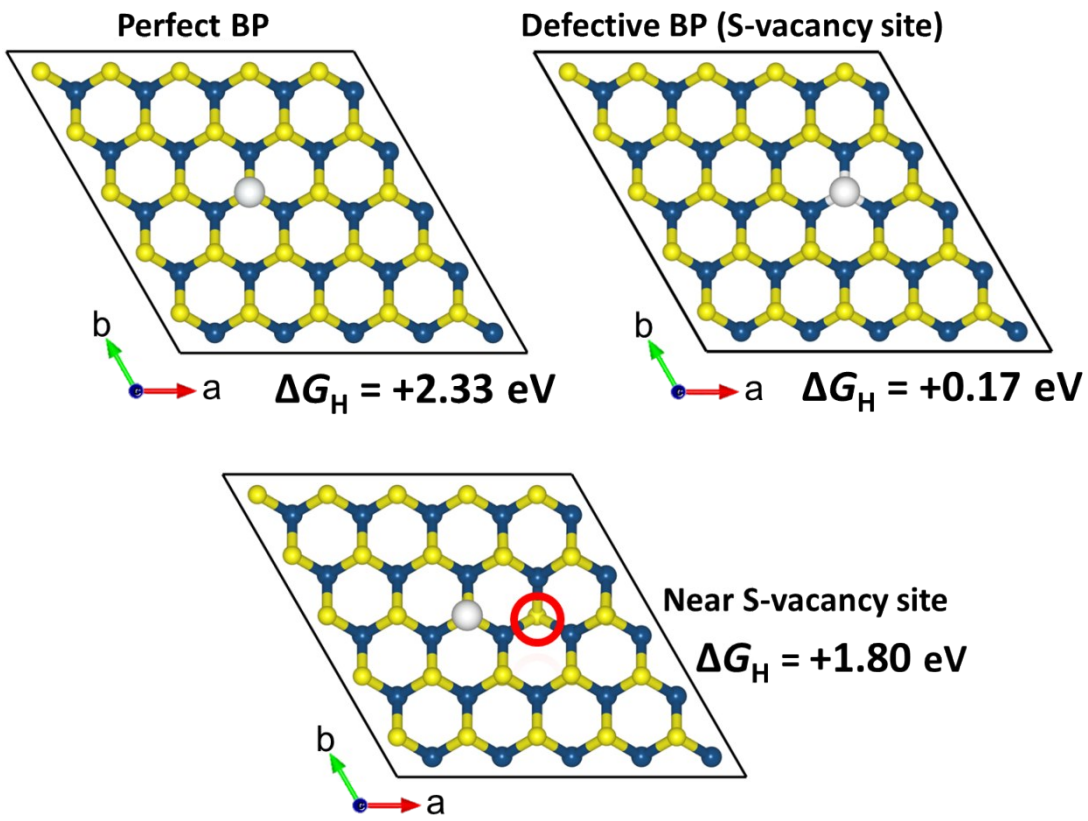

Figure S22. Calculated Gibbs free energy for hydrogen adsorption on perfect and defective (S-vacancy site) WS_2 basal (0001) plane (BP).

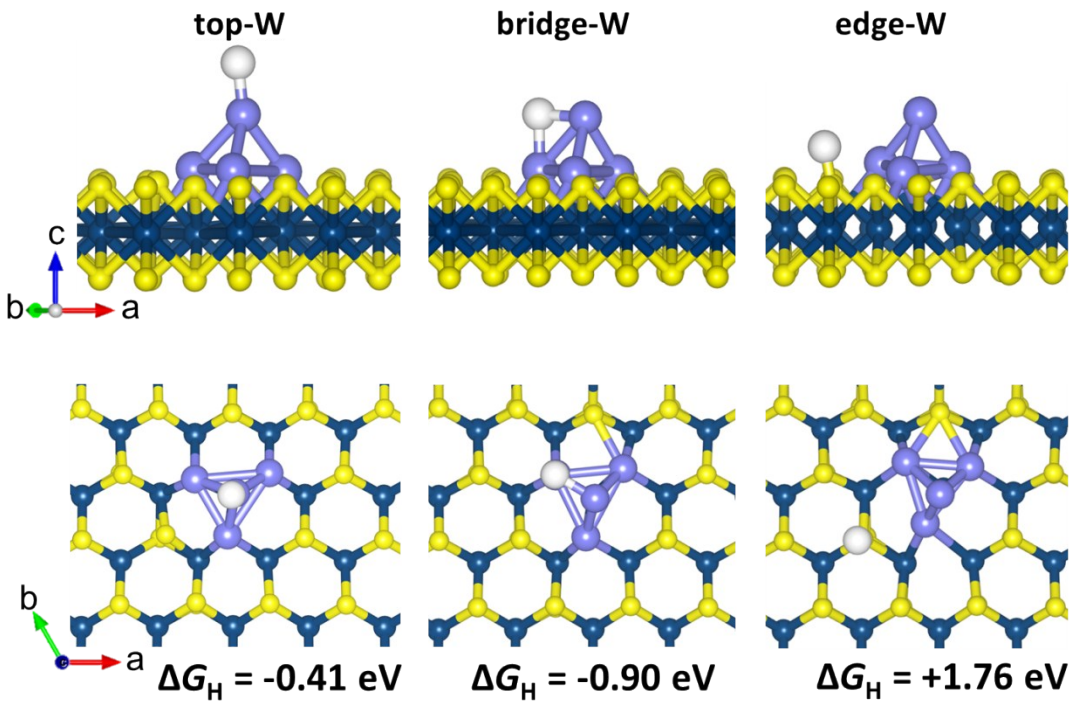

Figure S23. Calculated Gibbs free energy for hydrogen adsorption on the probable adsorption sites of a tetrahedron W cluster on the defective WS_2 basal plane (BP).

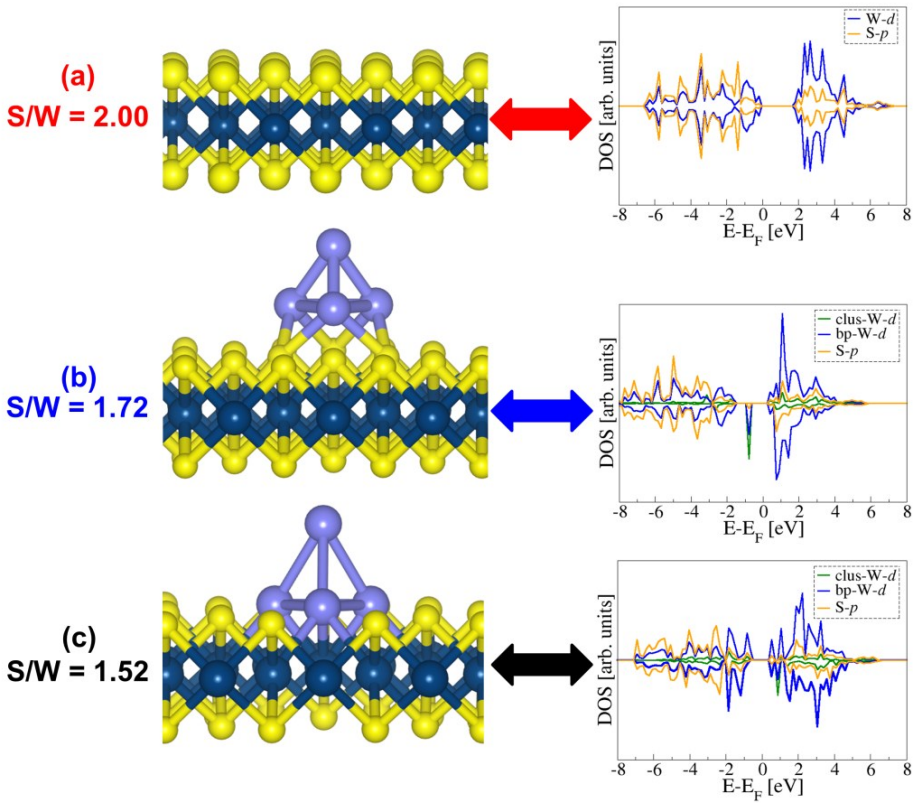

Figure S24. The partial density of states (PDOS) of (a) perfect WS_2, (b) W-cluster on perfect WS_2, and (c) W-cluster on defective WS_2.

References

1. A. R. Kucernak and C. Zalitis, *J. Phys. Chem. C*, 2016, **120**, 10721-10745.
2. J. D. Benck, T. R. Hellstern, J. Kibsgaard, P. Chakthranont and T. F. Jaramillo, *ACS Catal.*, 2014, 3957-3971.
3. A. P. Murthy, J. Theerthagiri and J. Madhavan, *J. Phys. Chem. C*, 2018, **122**, 23943-23949.
4. T. Shinagawa, A. T. Garcia-Esparza and K. Takanabe, *Sci. Rep.*, 2015, **5**, 13801.
5. D. Voiry, H. Yamaguchi, J. Li, R. Silva, D. C. B. Alves, T. Fujita, M. Chen, T. Asefa, V. B. Shenoy, G. Eda and M. Chhowalla, *Nat. Mater.*, 2013, **12**, 850-855.
6. J. Yang, D. Voiry, S. J. Ahn, D. Kang, A. Y. Kim, M. Chhowalla and H. S. Shin, *Angew. Chem. Int. Ed.*, 2013, **52**, 13751-13754.
7. L. Cheng, W. Huang, Q. Gong, C. Liu, Z. Liu, Y. Li and H. Dai, *Angew. Chem. Int. Ed.*, 2014, **53**, 7860-7863.
8. J. Duan, S. Chen, B. A. Chambers, G. G. Andersson and S. Z. Qiao, *Adv. Mater.*, 2015, **27**, 4234-4241.
9. Z. Wu, B. Fang, A. Bonakdarpour, A. Sun, D. P. Wilkinson and D. Wang, *Appl. Catal. B: Environ.*, 2012, **125**, 59-66.